2nd August 2023

Understanding Transient Ionic Diode Currents and Impedance Responses for Aquivion® Coated Microholes

Evaldo Batista Carneiro-Neto [1,2], Zhongkai Li [1], Ernesto Pereira [2], Klaus Mathwig [3], Philip J. Fletcher [4], Frank Marken *[1]

[1] *Department of Chemistry, University of Bath, Claverton Down, Bath BA2 7AY, UK*

[2] *Department of Chemistry, Federal University of São Carlos, Rod. Washington Luiz, Km 235, CEP 13565-905, São Carlos, SP, Brazil*

[3] *imec within OnePlanet Research Center, Bronland 10, 6708 WH Wageningen, The Netherlands*

[4] *University of Bath, Materials & Chemical Characterisation Facility MC², Bath BA2 7AY, UK*

To be submitted to ACS Applied Materials and Interfaces

Proofs to F. Marken (F.Marken@bath.ac.uk)

Abstract

Ionic diode-based devices or circuits can be applied, for example, in electroosmotic pumps or in desalination processes. Aquivion® ionomer coated asymmetrically over a Teflon film (5 μm thickness) with a laser-drilled microhole (approx. 10 μm diameter) gives a cationic diode with a rectification ratio of typically 10 to 20 (measured in 0.01 M NaCl with ±0.3 V applied bias). Steady state voltammetry, chronoamperometry, and electrochemical impedance spectroscopy data are employed to characterise the ionic diode performance parameters. Next, a COMSOL 6.0 finite element model is employed to quantitatively assess/compare transient phenomena and to extract mechanistic information by comparison with experimental data. The experimental diode time constant and diode switching process associated with a distorted semi-circle (with a typical diode switching frequency of 10 Hz) in the Nyquist plot are reproduced by computer simulation and rationalised in terms of microhole diffusion-migration times. Fundamental understanding and modelling of the ionic diode switching process can be exploited in the rational/optimized design of new improved devices.

Keywords: ionic diode; desalination; diffusion-migration; accumulation-depletion; electrochemical impedance spectroscopy

1. Introduction

Ionic diodes are asymmetrically ion conductive devices based on nanopores,[1,2] nanocones,[3,4,5,6] micro-/nano-fluidic systems,[7] or based on microhole devices.[8] By combining or coupling ionic diodes into ionic circuits,[9] AC electricity can be employed to drive processes such as electroosmosis[10] or water desalination avoiding side reactions at capacitive driver electrodes.[11] Characteristic properties for ionic diodes are linked to the rectification ratio (the ratio of currents in "open" and "closed" states) and the time constant for switching of the diode state. The rectification ratio (as a function of applied voltage) is obtained experimentally, for example by voltammetry under close to steady state conditions. In contrast, the diode switching time constant is a transient property accessible for example with chronoamperometry or with electrochemical impedance spectroscopy. For ionic diodes based on a Nafion ionomer film on a 10 μm diameter microhole, diode switching frequencies of typically f_{diode} = 10 Hz were

observed from the "summit frequency" of depressed semi-circular features in the Nyquist representation.[12] This can be translated into a corresponding diode time constant with $\tau_{diode} = 1/\omega_{diode} = 1/(2\pi f_{diode})$ = 16 ms in this case. Although electrochemical impedance spectroscopy studies have been previously reported for microhole ionic diodes, there has been no full analysis of the impedance data in terms of physical parameters such as concentration profile changes linking to diode time constant and diode frequency. It is reported here that the finite element simulation approach allows diode time constant and frequency parameters to be better understood.

In this report, the ionomer Aquivion® from Solvay (commonly applied in fuel cells and electrolysers[13,14]) has been selected for the assembly of ionic diodes on a 5 μm thickness Teflon substrate with a laser-drilled microhole (approx. 10 μm diameter). Aquivion® offers good conductivity[15] and opportunities for additive device manufacturing.[16] Previously, films of ion conducting materials such as cellulose,[17] M13 phage,[18] nanocarbons,[19] graphene oxide,[20] or polyacrylonitrile[21] have been employed in ionic diodes. The charge density of Aquivion® (designed for fuel cell[22] and energy applications[23,24]) is relatively high (approx. $[-e^-]$ = 1.16 mol dm^{-3} or -112000 C dm^{-3}) to provide high cation conductivity whilst retaining processability and chemical stability. Figure 1A shows the operational principle based on a highly cation-conductive ionomer film asymmetrically deposited over the microhole in a Teflon substrate. Depending on the applied bias potential, either accumulation or depletion of aqueous electrolyte within the microhole region occurs leading to the observation of "open" and "closed" diode states, respectively.

Multi-physics finite element computational models provide powerful tools for the simulation of electrochemical processes and data.[25] From a modelist perspective, the ionic diode devices can be described by the simultaneous solution of the Nernst-Planck-Poisson equations with appropriate boundary conditions. This approach has been employed previously for example to investigate the ion current rectification in nanopores[26] or the ion transport through charged conical micropores,[27] and for the ion transport in asymmetric ionomer film deposits over microholes.[28] For the latter case, previous studies have been limited to steady state current data. Here, the transient current components and electrochemical impedance spectroscopy data are investigated. It is shown that the computer simulation model can reproduce the experimental

data without the need to invoke non-physical equivalent circuit models (these are used here only for comparison of data sets).

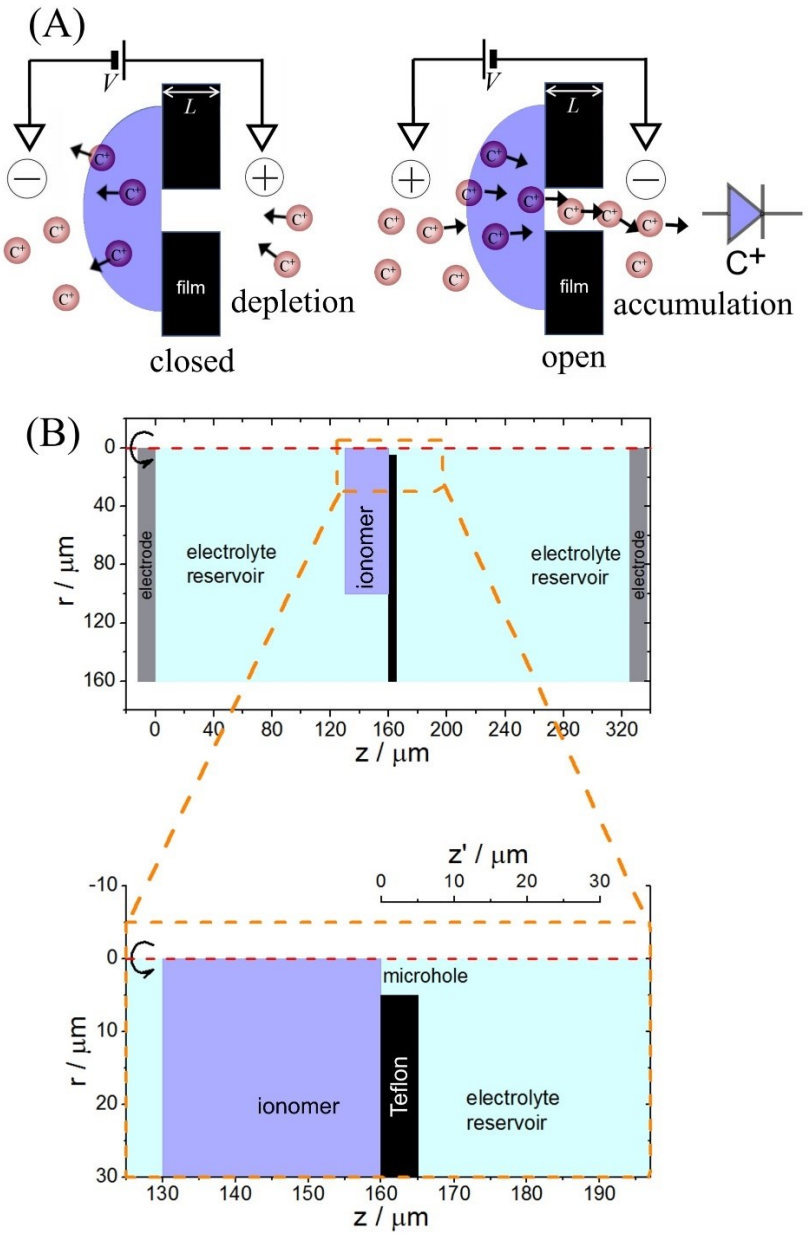

Figure 1. Representation of (A) the diode switching process and (B) the geometry employed in multi-physics simulations. Due to the symmetry around the axial axis (red dashed line) of the system, only a 2D model was considered (shown here as cross-section of half of the cell = the asymmetric unit). The region contained inside the orange dashed rectangle is enlarged below to show the details of the microhole. The internal ionomer|water interface is defined as the starting point of the axis *z'* (used later to represent the profile of the sodium concentration).

In this report, the processes in a cationic diode based on Aquivion® coated 30 μm thick over an approx. 10 μm diameter microhole in 5 μm thick Teflon are investigated. Both steady state and transient currents (voltammetry, chronoamperometry, electrochemical impedance spectroscopy) are investigated. Comparison of the finite element model with experimental data suggests that diffusion-migration processes in the microhole region determine the diode time constant.

2. Experimental

2.1. Chemical Reagents. Aquivion® D98-25BS (25% w/w in water; eq. wt. 980 g/mol SO_3H; density 1.14 g cm^{-3}; approx. charge concentration 1.16 mol dm^{-3}) was purchased from Sigma-Aldrich. Absolute ethanol (99.97%) was purchased from VWR Chemicals. Sodium chloride (99.5%) was purchased from Fisher Scientific Ltd. Agarose powder was purchased from Melford Ltd. All chemicals were utilised as received without further purification. Aqueous solutions were prepared using ultra-pure water from a Thermo Scientific water purification system, with a resistivity not less than 18.2 MΩ cm (20 ± 2°C). The pH of 0.01 M NaCl was 6.9 ± 0.1.

2.2. Instrumentation. Electrochemical measurements were performed with a 4-electrode configuration on a computer-controlled Ivium Technologies CompactStat potentiostat for cyclic voltammetry, chronoamperometry, and for electrochemical impedance spectroscopy. The electrochemical cell contained two cylindrical half-cells, which were separated by a Teflon thin film (5 μm thick) with a laser-drilled microhole of 10 μm diameter (see Figure 2; Laser Micromachining Ltd., St. Asaph, LL17 0JG, UK). The microhole region was coated asymmetrically with an Aquivion® membrane. Briefly, the Teflon film was placed onto 1% agarose gel to allow Aquivion® solution (20% v/v dilution of Aquivion® solution in ethanol) to be applied from one side only. Once the ionomer film was dry, the modified Teflon film was peeled off the gel and used in electrochemical measurements. Figure 2 shows typical scanning electron microscopy images with EDX elemental mapping for the Teflon film with microhole and Aquivion® film underneath. Image 2C corresponds to the fluorine elemental distribution with Teflon dominating. Image 2D shows the carbon elemental map with a stronger signal for Aquivion® compared to that for Teflon. In contrast, Figure 2E shows that oxygen is more

abundant in Aquivion®. Figure 2F shows the experimental configuration for electrochemistry. Carbon rods of 1 mm diameter served as both working and counter electrodes, and silver wires (0.5 mm diameter) were applied as quasi-sense and quasi-reference electrodes. The symmetry of the system (with electrolyte solutions) ensured that the silver quasi-reference electrodes are always at equal potential. Silver quasi-reference electrodes help avoiding artefacts in impedance data due to frits in commercial reference electrodes. During all measurements, the working and sense electrodes were placed on the membrane side of the cell. Scanning electron microscopy (SEM) and energy-dispersive X-ray spectroscopy (EDX) were performed on a Hitachi SU390 variable pressure SEM with attached Oxford Instruments Ultim Max 170 mm^2 EDX detector for the microhole imaging, and on a Jeol JSM-7900F field emission SEM with attached Oxford Instruments Ultim Extreme 100 mm^2 windowless EDX analyser for the cross-section imaging.

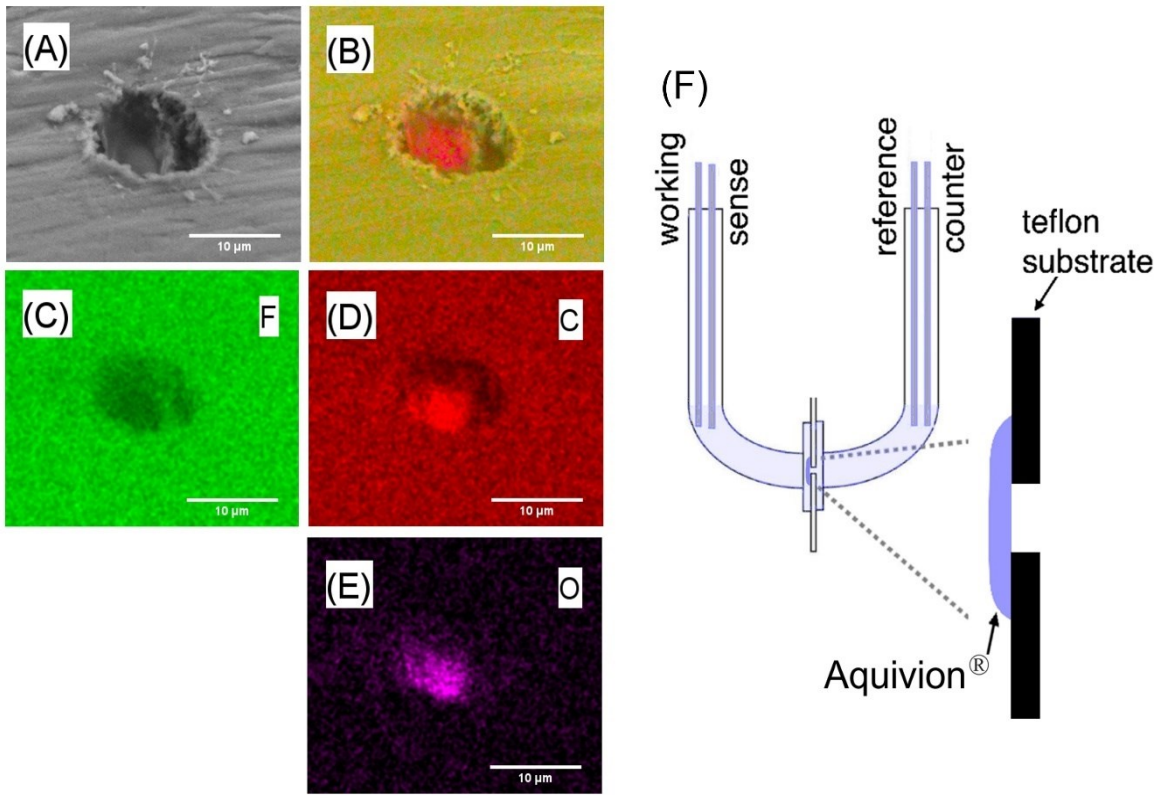

Figure 2. (A) Scanning electron microscopy (SEM, secondary electron) images of the backside of Aquivion®-coated Teflon film with 10 µm microhole. (B-E) EDX mapping for F (mainly in Teflon), C and O (mainly in Aquivion®). Image (B) is layered EDX images combing (C-E). (F) Schematic of the experimental 4-electrode cell for voltammetry and for electrochemical impedance spectroscopy experiments. The ionomer is on the working electrode side.

2.3. Procedures

Membrane preparation. A 20% v/v dilution of Aquivion® solution in ethanol was prepared to create a similar ionomer concentration to the previously reported studies on Nafion diodes.[12] The Teflon film was placed on an agarose gel substrate to prevent the ionomer solution from penetrating through the microhole. A volume of 10 µL of the solution was then deposited onto the microhole region of the Teflon film to form a membrane by drop-casting. For SEM and EDX analysis, Aquivion® membranes prepared with this methodology were coated with 5 nm of chromium metal to improve electrical conductivity and remove charging. Cross-sectional SEM and EDX indicated an Aquivion® membrane thickness of typically 30 ± 5 µm (see Figure 3).

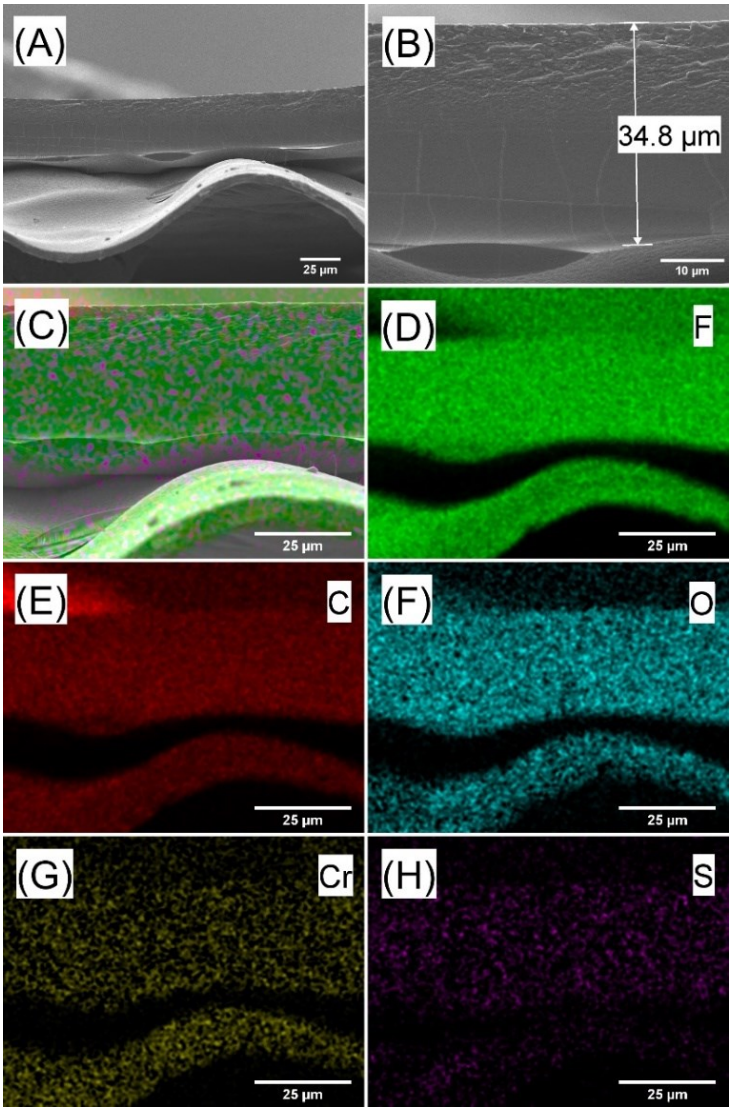

Figure 3. (A-B) Cross-section scanning electron microscopy (SEM, secondary electron, 5 nm chromium applied to suppress charging) images of a 5 μm Teflon film (approx. 5 μm thick) coated with Aquivion® membrane (approx. 30 μm thick). (C-H) EDX mapping for F, C, O, Cr and S. F is present in both materials but S and O are mainly located in Aquivion®. Image (C) is layered EDX images combing (D-H).

Electrochemical cell assembly. The electrochemical characterisation of the Aquivion® diode was performed in a "U-cell" with 4-electrode configuration (Figure 2F). A solution of aqueous 10 mM NaCl was placed into both reservoirs as electrolyte for performing cyclic voltammetry, chronoamperometry, and electrochemical impedance spectroscopy. The presence of the Aquivion® membrane coated asymmetrically on the microhole in Teflon is shown in Figure 2.

3. Finite Element Simulation

In the computer simulation (COMSOL Multiphysics 6.0) the two-dimensional axisymmetric ionic diode geometry (Figure 1B) is formed by two identical cylindrical reservoirs connected by a single microhole (due to axial symmetry, the simulation is possible in 2D using the asymmetric unit in Figure 1). Each reservoir has a radius of 160 μm and a height of 160 μm. The microhole has a length of 5 μm and a radius of 5 μm and is covered on one side with 30 μm thickness ionomer film which extends 100 μm radially. The reservoir and microhole spaces were filled with 10 mM NaCl solution (see parameters in Table 1). The ionomer film has a uniform fixed negative charge with assumed concentration of 0.05 mol dm^{-3}. This is lower compared to the Aquivion® charge density of approx. 1.16 mol dm^{-3} and a compromise to achieve convergence and to avoid a much finer meshing and substantial additional computational time requirements.

Electroneutrality is maintained in the electrolyte

$$c_{Na,e} - c_{Cl,e} = 0 \quad (1)$$

and inside the ionomer

$$c_{Na,mem} - c_{Cl,mem} - c_{mem} = 0 \quad (2)$$

Here, $c_{Na,e}$ and $c_{Cl,e}$ are the sodium cation and chloride anion concentrations in the electrolyte. The parameters $c_{Na,mem}$ and $c_{Cl,mem}$ denote the sodium cation and the chloride anion concentrations in the ionomer. The parameter c_{mem} describes the concentration of fixed negative charges (assumed to be anionic sulfonate groups) inside the ionomer. The electrolyte potential is described by the Laplace equation.

$$\varepsilon_r \, \varepsilon_0 \, \Delta\varphi \; = \; 0 \tag{3}$$

Here, ε_r is the relative dielectric constant which in this case is assumed to be 80, ε_0 is the vacuum permittivity constant, and φ is the local electrolyte potential. The distribution of concentrations inside the system is described by the Nernst-Planck equation.

$$J_{i,k} \; = \; - D_{i,k} \, \nabla c_{i,k} - \frac{z_{i,k} \, D_{i,k} \, F}{R \, T} \, c_{i,k} \, \nabla\varphi \tag{4}$$

$$\frac{\partial c_{i,k}}{\partial t} \; = \; - \nabla \cdot J_{i,k} \tag{5}$$

Here, $c_{i,k}$, $D_{i,k}$, and $z_{i,k}$ are, in this order, the flux density, the concentration, the diffusion coefficient, and the ionic charge of species i (*e.g.* Na^+ or Cl^-) in the domain k (*e.g.* electrolyte or ionomer layer). F and R have their usual meanings and T is the absolute temperature which in this case is 298.15 K.

At both ends of the domain (*e.g.* at $z = 0$ µm and at $z = 325$ µm for all r) it was assumed that both ionic concentrations were equal to the bulk concentration (*i.e.* $10\,mM$). A potential difference was applied between these external interfaces. The boundaries between the electrolyte and the ionomer film were defined with the Donnan potential condition, which considers the electrochemical potential to be the same on each side of the interface.

$$\varphi_e \; - \; \varphi_{mem} \; = \; - \frac{R \, T}{z_i \, F} \ln \frac{c_{i,e}}{c_{i,mem}} \tag{6}$$

Here, the subindexes e and mem refer to electrolyte or membrane, respectively. All the other boundaries were defined as null concentration flux and with zero surface charge. In all simulations, a first step was performed which consisted of solving the set of equations under steady-state condition and in the absence of applied potential. With this done, it was possible to calculate the equilibrium concentrations of sodium cations and chloride anions and the electric potential profile throughout the device with applied bias. Table 1 gives the important parameters with a brief description.

Table 1. Summary of parameters and associated values defined in the simulations.

Symbol	Value	Description
$D_{Na,e}$	$1.3 \times 10^{-9}\ m^2\ s^{-1}$ †	Diffusion coefficient of Na^+ in the electrolyte
$D_{Cl,e}$	$2.0 \times 10^{-9}\ m^2\ s^{-1}$ †	Diffusion coefficient of Cl^- in the electrolyte
$D_{Na,mem}$	$6.5 \times 10^{-11}\ m^2\ s^{-1}$ ‡	Diffusion coefficient of Na^+ in the membrane
$D_{Cl,mem}$	$8.4 \times 10^{-10}\ m^2\ s^{-1}$ ‡	Diffusion coefficient of Cl^- in the membrane
c_{mem}	$0.05\ mol\ dm^{-3}$ *	Concentration of fixed negative charge inside the membrane
$z_{i,k}$	± 1 *	Ionic charge for Na^+ and Cl^-

† from reference [29]
‡ parameters that are free; estimated in the impedance fitting process.
* parameters that are fixed in the simulations.

The current through the diode device is calculated by integration of the normal ionic flux over one of the ends of the domain. At the boundary $z = 325\,\mu m$ and for $0 \leq r \leq 160\,\mu m$ the expression below was employed to give the net current.

$$i = -F \int_0^{160\,\mu m} 2\,\pi\,(J_{Na} - J_{Cl}) r\,dr \tag{7}$$

The equations are solved employing the Finite Element Method (FEM, COMSOL Multiphysics 6.0). A mesh was built according to a predefined method with a maximum element size of $12\,\mu m$. At the interface between the electrolyte and the ionomer the maximum element size was $0.10\,\mu m$, except for the interface inside the microhole, where the maximum element size was $0.01\,\mu m$ and at the rim of the microhole, where the maximum element size was $10^{-4}\,\mu m$.

This was necessary to ensure an accurate calculation of the gradients in every region. The total mesh in the model was constituted by 119,508 elements. The computational time spent in each simulation was about 12 h (on a personal computer with a processor Intel$^{(R)}$ Core^{TM} I7-8700 with 6 cores working at 3.20 GHz and 32 GB of RAM memory).

4. Results and Discussion

4.1. Aquivion® Coated Microhole Diodes: Experimental Data

Typical cyclic voltammetry data for a 30 μm thick Aquivion® film on a 5 μm Teflon film with 10 μm diameter microhole are shown in Figure 4A for 10 mM NaCl electrolyte. With a potential scan rate of 0.2 Vs^{-1}, data are close to steady state, although a current loop is observed in the positive potential range. In the negative potential range, the ionic diode is closed, and currents remain low. In the positive potential range, accumulation of electrolyte in the microhole causes lower resistivity and higher currents (the diode is open). Three typical current traces for three repeat ionic diode devices are shown. The variation in the observed currents can be attributed to (i) variability in the laser drilling and shape of the microhole (see Figure 2), (ii) variability in the ionomer coating in terms of thickness and in terms of some penetration of ionomer into the microhole. Rectification ratio data was obtained by chronoamperometry at ±0.3 V (Figure 4B). Typical values range from 10 to 23. Perhaps interestingly, devices with the lower rectification ratio appears to be linked also to a faster switching time constant (*vide infra*).

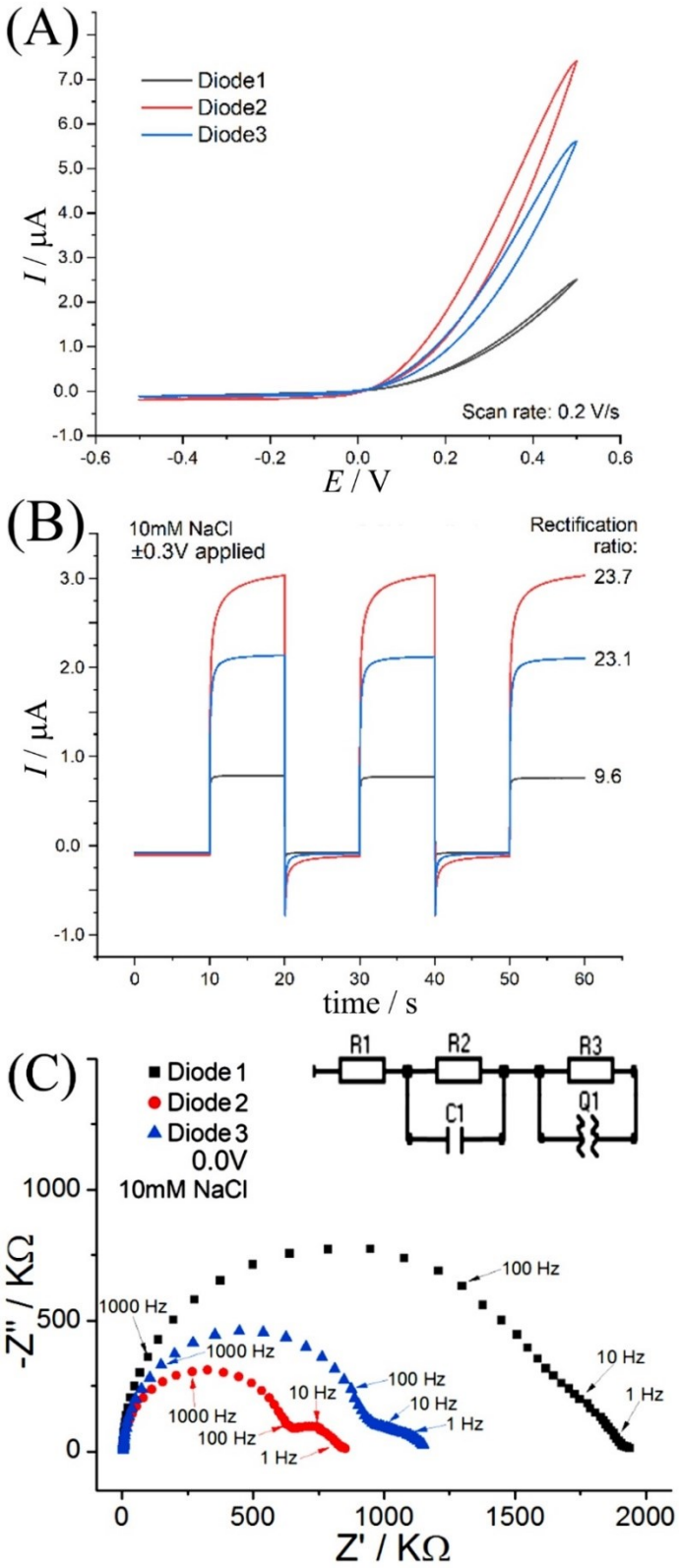

Figure 4. (A) Cyclic voltammograms (scan rate 0.2 Vs^{-1}) for three Aquivion® microhole diodes in 0.01 M NaCl aqueous solution. (B) Chronoamperometry transient currents for the diodes with applied pulses of ±0.3 V. (C) Electrochemical impedance data for the diodes with an amplitude of 25 mV, bias of 0.0 V and frequency range of 1 Hz to 100 kHz.

The analysis of the diode behaviour based on electrochemical impedance spectroscopy provides further quantitative detail. When performed in the closed state (negative potential range) or in the open state (positive potential range) the diode is essentially locked into low or high resistivity behaviour (not shown). However, with a bias potential of 0.0 V the diode switching process from open to closed can be further investigated. Data in Figure 4C shows typical Nyquist plots with all three devices showing a first (high frequency) and a second (low frequency) semi-circular feature. The higher frequency semicircle is associated with charging of the Teflon film. The lower frequency semicircle is associated with diode switching.

Table 2. Electrochemical impedance spectroscopy data (in 10 mM NaCl; bias 0.0 V; amplitude 25 mV) for three ionic diode devices. Given in brackets is the fitting error.

element	**units**	**Diode 1**	**Diode 2**	**Diode 3**
R1	KΩ	3.77 (±0.08)	3.92 (±0.07)	3.89 (±0.07)
R2	MΩ	1.49 (±0.01)	0.611 (±0.005)	0.900 (±0.004)
R3	KΩ	413 (±11)	227 (±6)	243 (±9)
C1	nF	0.44 (±0.002)	0.310 (±0.002)	0.420 (±0.002)
Q1	$s^N\Omega^{-1}$	6.7 (±0.3) × 10^{-8}	15.7 (±0.8) × 10^{-8}	32.6 (±1.6)×10^{-8}
N	dimensionless	0.783 (±0.008)	0.779 (±0.008)	0.700 (±0.008)

The impedance data can be fitted and represented (in first approximation, see Table 2) by an electric circuit model (Figure 4) based on a serial resistor (R1), a capacitor describing the charging of the Teflon film (C1), a resistor describing ion current flow through the ionomer and microhole region at high frequency and without concentration polarisation (R2), and a resistor (R3) constant phase element (Q1, N) representing the process of diode open/close switching. The electric circuit model fit is satisfactory to describe the behaviour of the system, but it lacks physical insight. It is better to approach the data interpretation with a physical finite element model avoiding the non-physical electric circuit model.

4.2. Aquivion® Coated Microhole Diodes: Computer Simulation of Steady State Phenomena

The finite element simulation approach was based on two free parameters, $D_{Cl,mem}$ and $D_{Na,mem}$, which were adjusted to give a satisfactory match in impedance data (*vide infra*). Figure 5 shows a simulated I-V curve in the range of $-0.5\,V$ to $0.5\,V$ simulated with a scan rate of 0.2 Vs^{-1}. The diode character and rectification effect are clearly observed (compare to Figure 4A). In the inset of Figure 5 the rectification ratio is plotted *versus* applied voltage (*e.g.* at ±0.3 V the rectification ratio is I(+0.3 V)/I(-0.3 V) = 2.5). The value increases from 1 to about 4, which is slightly lower when compared to the experimental data (mainly due to the lower charge density chosen in the simulated ionomer). This parameter is important as a measure of the efficiency of the rectification performance of the diode.

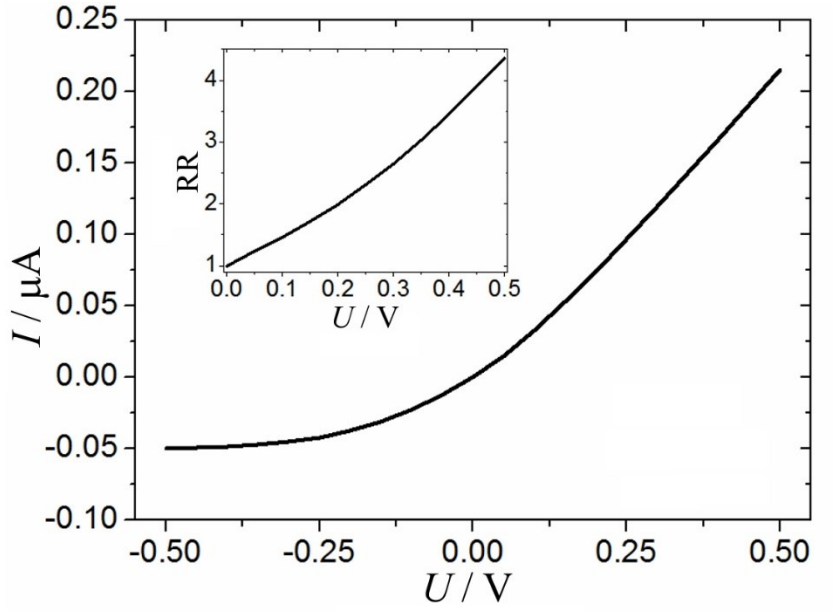

Figure 5. Simulated voltammetry of the ionic diode at 0.2 Vs^{-1}. Inset shows the rectification ratio (RR) as function of the applied voltage.

4.3. Aquivion® Coated Microhole Diodes: Computer Simulation of Transient Phenomena

Figure 6A shows the simulated current that flows through the device when the applied potential is switched between -0.3 V and +0.3 V. The transient currents are comparable to experimental transient data (Figure 4B, diode 2). The ratio of the current in the open state divided by the current in the closed state gives the rectification ratio (RR), which is 2.6 under these conditions. One of the advantages of the simulation is that it allows a deeper understanding of the system under investigation by access to local phenomena such as concentration profiles. Figure 6B shows a plot of the Na^+ concentration profile (the concentration is normalised relative to the

bulk concentration c^*_{Na+}) inside of the microhole versus the distance from the ionomer z' (see Figure 1). Due to electroneutrality Na^+ and Cl^- concentrations are equal. At a time t = 39 s (Figure 6C; closed diode; black line) depletion occurs and the electrolyte is removed from the microhole region. In contrast, at a time t = 41 s (Figure 6C; open diode; green line) electrolyte is accumulated inside of the microhole. Note that the parameter z' represents the distance from the ionomer surface inside of the microhole. Both, the gradual rise in current when switching the diode open and the negative current spike when switching the diode to closed are associated with electrolyte entering the microhole region (accumulation) and electrolyte being removed from the microhole region (depletion).

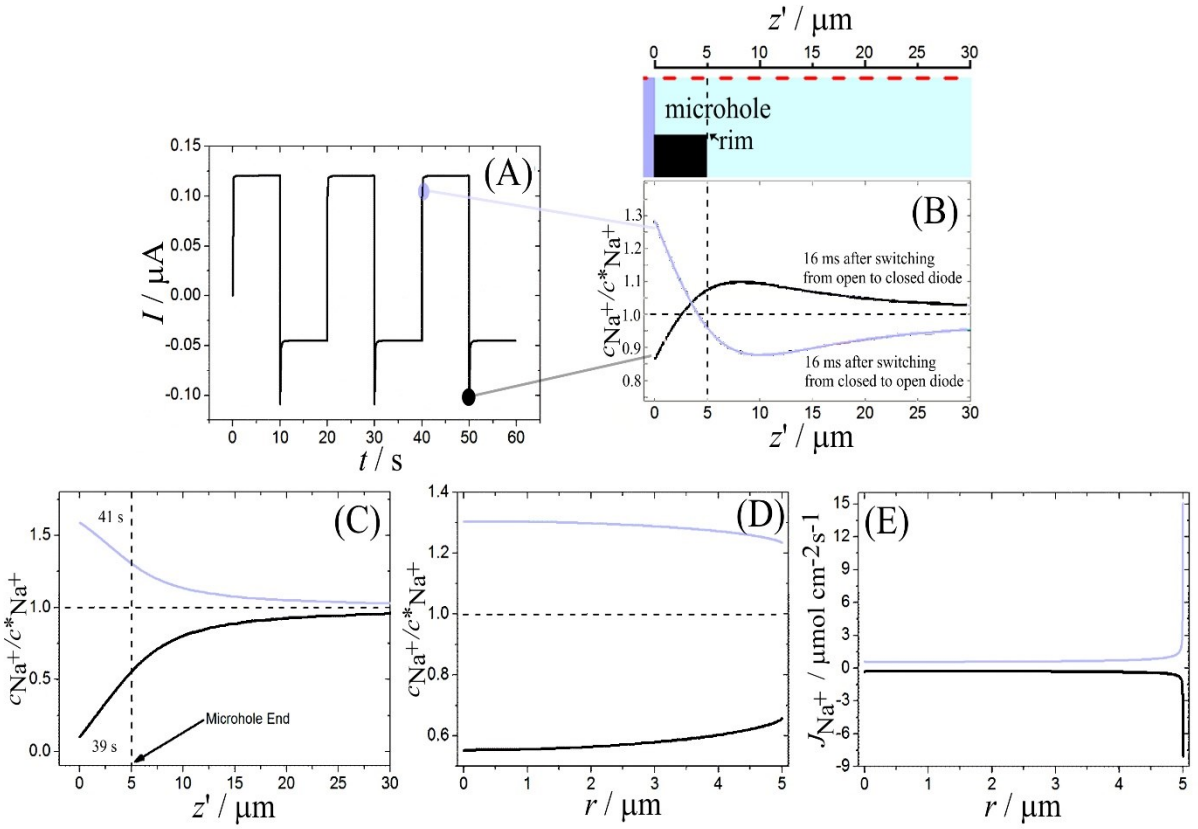

Figure 6. (A) Chronoamperometry data simulated for a single microhole diode for ±0.3 V. (B) during the transient response: Na^+ concentration profile sampled at 16 ms after switching from closed to open (green) and at 16 ms after switching from open to closed (black). (C) At quasi-steady state: Na^+ concentration profile at 39 s (closed diode, black) and at 41 s (open diode, green). The dashed line indicates the rim of the microhole. (D) Plot of Na^+ concentration (at 39 s and at 41 s) as a function of radius at the microhole rim z' = 5 µm. (E) Normal flux of Na^+ as a function of r at the rim of the microhole.

It is possible to explore the exact moment when switching from one diode state to another occurs. Figure 6B shows the Na^+ concentration profile 16 ms after switching from closed to open (green) and 16 ms after switching from open to closed (black). This is the moment when the net concentration of Na^+ integrated over the microhole region is equal to the bulk electrolyte concentration. For a 10 mm diameter microhole, the diode time constant $\tau_{diode} = 1/\omega_{diode} = 1/(2\pi f_{diode}) = 16$ ms can be estimated from the electrochemical impedance spectroscopy data (*vide infra*). The corresponding currents are indicated in Figure 6A as ±100 nA.

Figure 6D shows the Na^+ concentration profile radially at the location of the rim of the microhole. The switch from depletion (39 s, red) to accumulation (41 s, green) is clearly observed. The microhole geometry produces very high fluxes at the rim of the microhole (comparable to the situation of high current densities at the edge of microelectrodes.[30] Figure 6E shows the flux of Na^+ at the rim of the microhole and as a function of radius. For both accumulation (open diode) and depletion (closed diode) the effect of high flux at the edge is clearly observed.

4.4. Aquivion® Coated Microhole Diodes: Computer Simulation of Electrochemical Impedance Phenomena

Next, electrochemical impedance spectroscopy data are simulated for applied bias 0 V and for an amplitude 25 mV (peak-to-peak). The first semi-circular feature in the experimental data (Figure 4C) is due to charging of the Teflon film and therefore not part of the computer simulation model. The R2-C1 component of the equivalent circuit was subtracted from the experimental data to leave the second semi-circular feature to be reproduced with the finite element simulation model. The resistors R1 and R2 also are not accessible in the simulation model and therefore adjusted here with an arbitrary resistor R0.

Table 1 summarises all the parameters employed in the simulation with only two “free” parameters: the Na^+ diffusion coefficient in the ionomer membrane and the Cl^- diffusion coefficient in the ionomer membrane. Both of these free parameters were manually adjusted to generate a satisfactory fit of the simulation data with the experimental data. Figure 7 shows the comparison of simulation and experimental data for diode 2. Values optimised for the free

parameters were $D_{\mathrm{Na,mem}} = 6.5 \times 10^{-11}\, m^2\, s^{-1}$ and $D_{\mathrm{Cl,mem}} = 8.4 \times 10^{-10}\, m^2\, s^{-1}$. These values are physically plausible (but potentially impacted on by the too low charge density chosen for the ionomer in the simulation, *vide supra*), but inconsistent with earlier estimates for Nafion.[31] In the low frequency limit, the simulation model is flawed due to the limited reservoir size of only 160 μm. However, most of the data fits well confirming that the simulation does indeed reflect the conditions in the switching ionic diode. Note the "summit frequency" or diode frequency at approx. 10 Hz for both experiment and simulation. Summarised in Table 3 are equivalent circuit fitting parameters to compare both the experimental and the simulation data.

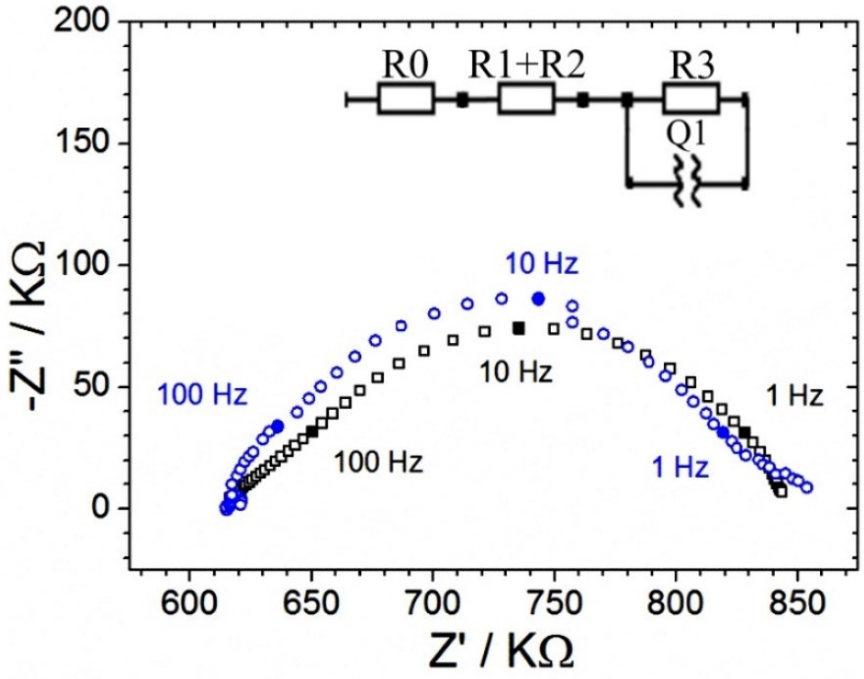

Figure 7. Nyquist representation of the simulated electrochemical impedance from 0.1 Hz to 10 kHz with 25 mV amplitude (black circles). Experimental data for the second "depressed" semi-circular feature of diode 2 (blue circles). Inset shows the parameters fitted to the experimental data (blue) and the parameters fitted to the simulated data (black) to compared data sets (circuit shown as inset).

Table 3. Electrochemical impedance spectroscopy data (in 10 mM NaCl; bias 0.0 V; amplitude 25 mV) summarised in terms of equivalent circuits for ionic diode 2 (for the second semi-circular feature) comparing experiment and COMSOL fitting.

Circuit element	**units**	**Diode 2: experiment**	**Diode 2: COMSOL fitting**
R0	MΩ	-	-2.86
R1+R2	MΩ	0.61	3.48
R3	KΩ	227	229
Q1	$s^{N}\Omega^{-1}$	15.7×10^{-8}	22.9×10^{-8}
N	dimensionless	0.779	0.707

Figure 8 shows the simulated sodium cation concentration profiles (normalised) over the axial and radial coordinates. Figures 8A and 8B show the concentration fluctuation along the *z*' axis for a frequency of 1 Hz (see Figures 8C and 8D for 10 Hz data). At 1 Hz, the concentration profile is in phase with the perturbation in potential, which indicates that the diode is always close to steady state. When the frequency is increased to 10 Hz, the changes in the concentration profile are smaller than the previous frequency, and they are no longer in phase with the perturbation in potential. In fact, at the diode frequency f_{diode} of the semi-circular feature, at 10 Hz, a maximum phase angle is observed.

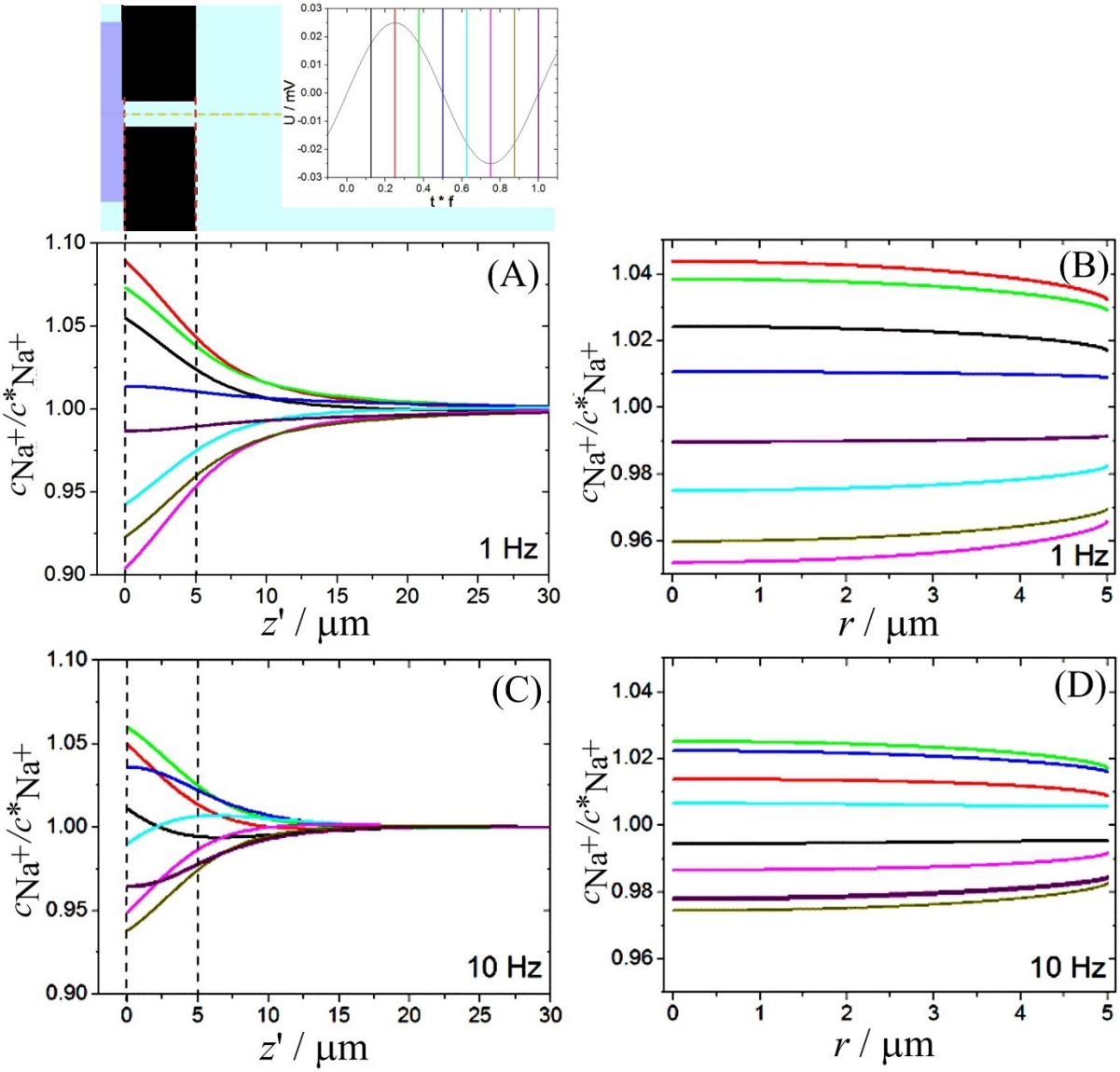

Figure 8. (A) Concentration profiles for Na^+ sampled at the centre of the microhole in the axial direction from the interface between the ionomer film and the electrolyte ($z' = 0$). The dashed line indicates the rim of the microhole. (B) Na^+ concentration profiles at the ionomer surface (z' = 5 µm) at the rim of the microhole filled with electrolyte; frequency 1 Hz. (C) Concentration profiles versus z' at 10 Hz. (D) Na^+ concentration profiles versus r. Insert: Each curve represents a fraction of the period ($\frac{1}{f}$) related by colours $\frac{1}{8f}$ (black), $\frac{1}{4f}$ (red), $\frac{3}{8f}$ (green), $\frac{1}{2f}$ (blue), $\frac{5}{8f}$ (cyan), $\frac{3}{4f}$ (magenta), $\frac{7}{8f}$ (dark yellow), $\frac{1}{f}$ (purple).

Figure 9 shows Bode plots of data from the experiment (A) and from the simulation (B). The peak in the phase angle plot (consistent with the point of inflection in the |Z| plot) represents the point in the frequency domain for which diode switching decouples from the excitation signal (going to higher frequencies). The "summit frequency" in the Nyquist representation can

therefore be understood as the frequency at which the diode switching becomes effective (going to lower frequencies).

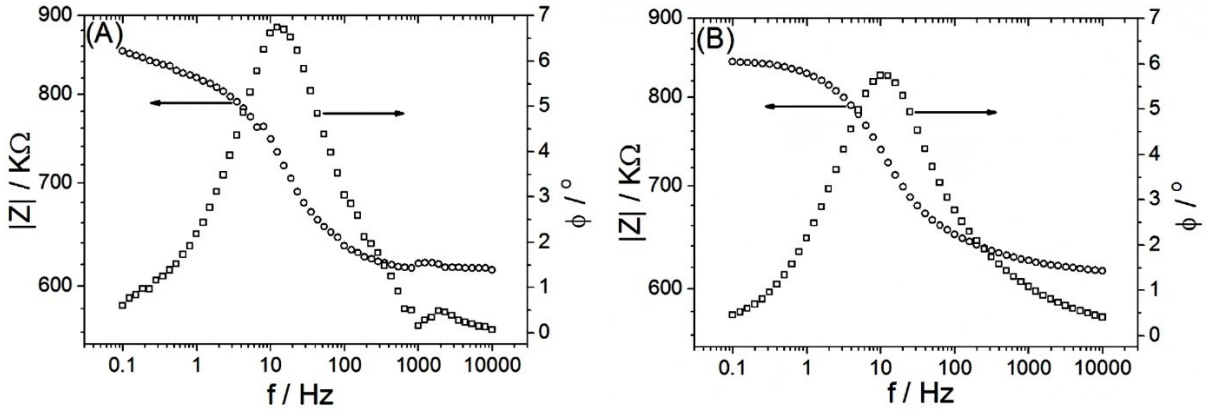

Figure 9. Bode plot for (A) experimental data and (B) simulation data. The summit frequency is consistent with the peak in the phase angle spectrum.

Therefore, both the "summit frequency" f_{diode} in the Nyquist representation (diode frequency) and the corresponding time constant of the semi-circular feature with $\tau_{diode} = 1/\omega_{diode} = 1/(2\pi f_{diode})$ describe the flux of electrolyte into and out of the microhole region. The time constant τ_{diode} can be understood as the point in time where a switch between accumulation and depletion occurs and the characteristic diode frequency f_{diode} represents the point in the frequency domain with maximum phase shift.

5. Conclusions

Transient currents and electrochemical impedance spectroscopy applied to ionic diode processes for microhole devices have been investigated with a finite element computer modelling approach. Rectification phenomena have been reproduced and ionic diode time constant and diode frequency have been discussed in terms of physical processes and parameters. Results lead to a deeper understanding of the diode function be revealing ion concentrations as a function of time and space in the microhole during potential switching. The diode switching and the diffusion-migration of electrolyte ions is quantitatively reproduced and the corresponding impedance spectroscopy data from experiment and from theory are in good agreement. This approach quantitatively links data to physical phenomena, and it goes beyond

the conventional use of circuit elements to fit impedance spectroscopy data. It is now possible to explore ionic diode performance at the level of theory to predict avenues for performance improvement.

In the future, better finite element models will be possible with higher resolution meshing to provide a better modelling of the ionomer | electrolyte interface and to better reflect the true charge density in ionomer materials and processes within the ionomer film. These models will provide theoretical tools to predict ionic diode performance and to explore performance of coupled ionic diodes, applied for example in the effective low energy desalination of sea water. These models will also allow a better comparison of different competing ionomer materials in the context of this application.

Acknowledgements

E.B.C.N. and E.P. acknowledge support from FAPESP (São Paulo Research Foundation, Grant Numbers 2013/07296-2, 2021/03592-2, 2022/06229-9), Shell, and the strategic importance of the support given by ANP (Brazil's National Oil, Natural Gas and Biofuels Agency) through the R&D levy regulation, CNPq (Grant Number 407878/2022), and CAPES (Code 001). F.M. thanks for the initial financial support by the EPSRC (EP/K004956/1).

References

(1) Lan, W.J.; Edwards, M.A.; Luo, L.; Perera, R.T.; Wu, X.J.; Martin, C.R.; White, H.S. Voltage-Rectified Current and Fluid Flow in Conical Nanopores. *Acc. Chem. Res.* **2016**, *49* (11), 2605 – 2613.

(2) Hou, X.; Guo, W.; Jiang, L. Biomimetic Smart Nanopores and Nanochannels. *Chem. Soc. Rev*. **2011**, *40* (5), 2385 – 2401.

(3) Cervera, J.; Schiedt, B.; Ramírez, P. A Poisson/Nernst-Planck Model for Ionic Transport through Synthetic Conical Nanopores. *Europhys. Lett.* **2005**, *71* (1), 35.

(4) Guo, W.; Tian, Y.; Jiang, L. Asymmetric Ion Transport through Ion-Channel-Mimetic Solid-State Nanopores. *Acc. Chem. Res.* **2013**, *46* (12), 2834 – 2846.

(5) Cai, J.; Ma, W.; Xu, L.; Hao, C.; Sun, M.; Wu, X.; Colombari, F.M.; de Moura, A.F.; Silva, M.C.; Carneiro-Neto, E.B.; Chaves Pereira, E.; Kuang, H.; Xu, C. Self-

assembled Gold Arrays that allow Rectification by Nanoscale Selectivity. *Angew. Chem. Inter. Ed.* **2019**, *58* (48), 17418 – 17424.

(6) Yossifon, G.; Chang, Y.C.; Chang, H.C. Rectification, Gating Voltage, and Interchannel Communication of Nanoslot Arrays due to Asymmetric Entrance Space Charge Polarization. *Phys. Rev. Lett.* **2009** *103* (15), 1 – 4.

(7) Cheng, L.J.; Guo, L.J. Nanofluidic Diodes. *Chem. Soc. Rev.* **2010**, *39* (3), 923 – 938.

(8) Putra, B.R.; Tshwenya, L.; Buckingham, M.A.; Chen, J.Y.; Aoki, K.J.; Mathwig, K.; Arotiba, O.A.; Thompson, A.K.; Li, Z.K.; Marken, F. Microscale Ionic Diodes: an Overview. *Electroanalysis* **2021**, *33* (6), 1398 – 1418.

(9) Li, Z.K.; Mathwig, K.; Arotiba, O.A.; Tshwenya, L.; Neto, E.B.C.; Pereira, E.C.; Marken, F. Driving Electrochemical Membrane Processes with Coupled Ionic Diodes. *Curr. Opinion Electrochem*. **2023**, *39*, 101280.

(10) Experton, J.; Wu, X.J.; Martin, C.R. From Ion Current to Electroosmotic Flow Rectification in Asymmetric Nanopore Membranes. *Nanomaterials* **2017**, *7* (12), 445.

(11) Li, Z.K.; Pang, T.T.; Shen, J.J.; Fletcher, P.J.; Mathwig, K.; Marken, F. Ionic Diode Desalination: Combining Cationic Nafion and Anionic Sustainion Rectifiers. *Micro Nano Engineer*. **2022**, *16*, 100157.

(12) He, D.P.; Madrid, E.; Aaronson, B.D.B.; Fan, L.; Doughty, J.; Mathwig, K.; Bond, A.M.; McKeown, N.B.; Marken, F. A Cationic Diode based on Asymmetric Nafion Film Deposits. *ACS Appl. Mater. Interfaces* **2017**, *9* (12), 11272 – 11278.

(13) Primachenko, O.N.; Marinenko, E.A.; Odinokov, A.S.; Kononova, S.V.; Kulvelis, Y.V.; Lebedev, V.T. State of the Art and Prospects in the Development of Proton-Conducting Perfluorinated Membranes with short Side Chains: A review. *Polym. Adv. Technol.* **2020**, *32* (4), 1386 – 1408.

(14) Sun, X.W.; Simonsen, S.C.; Norby, T.; Chatzitakis, A. Composite Membranes for High Temperature PEM Fuel Cells and Electrolysers: a Critical Teview. *Membranes* **2019**, *9* (7), 83.

(15) Mbarek, S.; El Kissi, N.; Baccouch, Z.; Iojoiu, C. Extrusion of Nafion and Aquivion Membranes: Environmentally Friendly Procedure and Good Conductivities. *Polymer Bull.* **2019**, *76* (3), 1151 – 1166.

(16) Trabia, S.; Olsen, Z.; Kim, K.J. Searching for a new Ionomer for 3D Printable Ionic Polymer-Metal Composites: Aquivion as a Candidate. *Smart Mater. Structures* **2017**, *26* (11), 115029.

(17) Aaronson, B.D.B.; Wigmore, D.; Johns, M.A.; Scott, J.L.; Polikarpov, I.; Marken, F. Cellulose Ionics: Switching Ionic Diode Responses by Surface Charge in Reconstituted Cellulose Films. *Analyst* **2017**, *142* (19), 3707 – 3714.

(18) Putra, B.R.; Szot-Karpinska, K.; Kudla, P.; Yin, H.; Boswell, J.A.; Squires, A.M.; Da Silva, M.A.; Edler, K.J.; Fletcher, P.J.; Parker, S.C.; Marken, F. Bacteriophage M13 Aggregation on a Microhole Poly(ethylene terephthalate) Substrate Produces an Anionic Current Rectifier: Sensitivity toward Anionic versus Cationic Guests. *ACS Appl. Bio Mater*. **2020**, *3* (1), 512 – 521.

(19) Tshwenya, L.; Marken, F.; Arotiba, O.A. Carbon Nanofibers Provide a Cationic Rectifier Material: Specific Electrolyte Effects, Bipolar Reactivity, and Prospect for Desalination. *ChemElectroChem* **2019**, *6* (12), 3145 – 3153.

(20) Putra, B.R.; Aoki, K.J.; Chen, J.Y.; Marken, F. Cationic Rectifier based on a Graphene Oxide-Covered Microhole: Theory and Experiment. *Langmuir* **2019**, *35* (6), 2055 – 2065.

(21) Tshwenya, L.; Marken, F.; Mathwig, K.; Arotiba, O.A. Switching Anionic and Cationic Semipermeability in Partially Hydrolyzed Polyacrylonitrile: a pH-Tunable Ionic Rectifier. *ACS Appl. Mater. Interfaces* 2020, *12* (2), 3214 – 3224.

(22) Breitwieser, M.; Bayer, T.; Buchler, A.; Zengerle, R.; Lyth, S.M.; Thiele, S. A Fully Spray-Coated Fuel Cell Membrane Electrode Assembly using Aquivion Ionomer with a Graphene Oxide/Cerium Oxide Interlayer. *J. Power Sources* **2017**, *351*, 145 – 150.

(23) Primachenko, O.N.; Marinenko, E.A.; Odinokov, A.S.; Kononova, S.V.; Kulvelis, Y.V.; Lebedev, V.T. State of the Art and Prospects in the Development of Proton-Conducting Perfluorinated Membranes with Short Side Chains: A Review. *Polymers Adv. Technol*. **2020**, *32* (4), 1386 – 1408.

(24) Sun, X.W.; Simonsen, S.C.; Norby, T.; Chatzitakis, A. Composite Membranes for High Temperature PEM Fuel Cells and Electrolysers: A Critical Review. *Membranes* **2019**, *9* (7), 83.

(25) Dickinson, E.J.F.; Ekstrom, H.; Fontes, E. COMSOL Multiphysics: Finite Element Software for Electrochemical Analysis. A Mini-Review. *Electrochem. Commun.* **2014**, *40*, 71 – 74.

(26) Wang, J.T.; Zhang, M.H.; Zhai, J.; Jiang, L. Theoretical Simulation of the Ion Current Rectification (ICR) in Nano-Pores based on the Poisson-Nernst-Planck (PNP) Model. *Phys. Chem. Chem. Phys*. **2014**, *16* (1), 23 – 32.

(27) Tao, Y.; Liu, W.Y.; Ren, Y.K.; Hu, Y.S.; Li, G.; Ma, G.Y.; Wu, Q.S. On Developing Field-Effect-Tunable Nanofluidic Ion Diodes with Bipolar, Induced-Charge Electrokinetics. *Micromachines* **2018**, *9* (4), 179.

(28) Mathwig, K.; Aaronson, B.D.B.; Marken, F. Ionic Transport in Microhole Fluidic Diodes based on Asymmetric Ionomer Film Deposits. *ChemElectroChem* **2018**, *5* (6), 897 – 901.

(29) Lide, D.R. (ed.) *CRC Handbook of Chemistry and Physics*, 74th ed., CRC Press, London, 1993-1994, p. 5-90.

(30) Tait, R.J.; Bury, P.C.; Finnin, B.C.; Reed, B.L.; Bond, A.M. An Explicit Finite-Difference Simulation for Chronoamperometry at a Disk Microelectrode in a Channel Flow Solution. *J. Electroanal. Chem.* **1993**, *356* (1-2), 25 – 42.

(31) Stenina, I.A.; Sistat, P.; Rebrov, A.I.; Pourcelly, G.; Yaroslavtsev, A.B. Ion Mobility in Nafion-117 Membranes. *Desalination* **2004**, *170* (1), 49 – 57.

Graphical Abstract